

State-to-state cross-sections for rotationally inelastic collision of LiH with Ne

Eryin Feng ^{a,b,*}, Wuyin Huang ^b, Zhifeng Cui ^b, Weijun Zhang ^a

^a *Laboratory of Environment Spectroscopy, Anhui Institute of Optics and Fine Mechanics, Chinese Academy of Sciences, Hefei 230031, PR China*

^b *Department of Physics, Anhui Normal University, Wuhu, Anhui 241000, PR China*

Received 7 February 2004; accepted 10 June 2004

Available online 6 July 2004

Abstract

The close coupling calculation of rotationally inelastic collision of Ne with LiH is first performed by employing a recently computed ab initio potential energy surface [Chem. Phys. Lett. 327 (2000) 305]. State-to-state differential, partial and integral cross-sections are calculated. Differential cross-sections show the feature of forward scattering for low Δj inelastic transitions and backward scattering for high Δj transitions. Two maxima exist in the curve of partial cross-sections and they are originated from different mechanism. The dependence of the integral cross-sections on j' for initial states $j = 0, 1$ displays a pronounced oscillatory structure rather than a monotonic one, and dependence on low collision energy presents resonance feature. These features are related to the anisotropic interaction potential.

© 2004 Elsevier B.V. All rights reserved.

Keywords: Rotationally inelastic cross-sections; Ne–LiH collision system; Close coupling calculations

1. Introduction

Collisional energy transfer in weakly interacting molecules has been the subject of numerous experimental and theoretical studies because of the importance of such processes in several areas of molecular physics and chemical physics. In particular, the relevant state-to-state cross-sections with which the actual energy content of the heat bath can be collisionally transferred to different molecular degrees of freedom, and the various external conditions which control the relative weights of the final inelastic channels, provide an essential piece of information.

Processes involving the LiH molecule have been of much interest in astrophysics and astrochemistry [1,2], because of its importance in lithium chemistry of early universe. The capability of accurately describing the interaction with some of the most abundant species like

rare gas obviously plays a significant role in understanding the formation of some of the “initial species”. Lots of attention has been devoted to the He–LiH system, which is a prototype one for studies both of intermolecular interaction potential and collision dynamics. The first calculation of He–LiH system was carried out by Silver [3] using the diagrammatic third Many Body Perturbation Theory. More recently, a set of calculations for this system were performed using different methods. Gianturco et al. [4] calculated the potential energy surface (PES) in the frame of the spin coupled Valence Bond theory, Taylor and Hinde [5] investigated this system based on the supermolecular ab initio techniques integrated with CCSD(T) treatment of electron correlation, Yan et al. [6] studied this system based on the MP4 theory and they eliminated the basis set superposition error. These calculations show that the basic features of the interaction in this system are essentially repulsive and orientationally anisotropic, owing to the highly polar property of the LiH target. Many quantum dynamics studies were performed on the basis

* Corresponding author. Tel.: +55-33-869-748; fax: +55-33-869-748.
E-mail address: fengbf@mail.ahnu.edu.cn (E. Feng).

of the PES mentioned above [7,8]. The results of the dynamics of the rotationally/rovibrationally inelastic collision can be reasonably explained from the feature of the PES.

For the Ar–LiH system, a model potential was derived [9] from the experimental cross-sections of LiH collision with Ar [10]. With this potential, Davies [11] made a close coupling (CC) calculation to obtain the rotationally inelastic degeneracy averaged and polarized cross-sections.

In contrast to He–LiH and Ar–LiH systems, the investigation of Ne–LiH is rare. The first work was performed by Shalabi et al. [12], in which they studied the interaction of Ne and LiH crystal surface and examined the binding energies. Recently, Xie and coworkers [13] calculated the potential energy surface for the rigid Ne–LiH system (fixed the distance of Li and H at its equilibrium value) using the MP4 theory with a large basis set, and with elimination of the basis set superposition error. The PES of Ne–LiH is also very anisotropic, similar to the PES of He–LiH. Two local potential minima are found, which locate at the linear Ne–LiH ($\theta = 180^\circ$) and at Ne–HLi ($\theta = 0^\circ$) geometry under Jacobi coordinates, respectively. They also calculated the vibrational energy levels using the vibrational SCF-CI method.

To the best of our knowledge, there are neither the experimental study nor the quantum dynamical study on the gaseous Ne–LiH reported in literature. In this paper, we report the results of the quantum dynamical investigation based on the Xie's PES for this system, and hope these results be useful for further experimental and theoretical studies. In the following section, we briefly review the potential energy surface and the quantum dynamics that used in our calculation, and then the state-to-state cross-sections and discussion are presented in detail in Section 3. Conclusions will be presented in Section 4.

2. Potential energy surface and computational method

2.1. Potential energy surface

Ab initio calculation of the interaction energy between Ne and LiH has been performed by Xie and coworkers in [13]. One hundred and fifty-six discrete points on the PES were fitted into an analytic expression, from which the details of this PES can be analyzed. In Fig. 1 we show the behavior of the potential as a function of the Ne–LiH separation for a number of relative orientations. The plot of equipotential energy contours is indicated in Fig. 2. The main features of the potential may be summarized below:

1. There are two local minima on the PES, the deeper one has an equilibrium distance of 2.47 Å at $\theta = 180^\circ$ (corresponding to the linear Ne–LiH) with a well depth of 206.13 cm^{-1} . The shallower one has an equilibrium distance of 4.97 Å at $\theta = 0^\circ$ (corre-

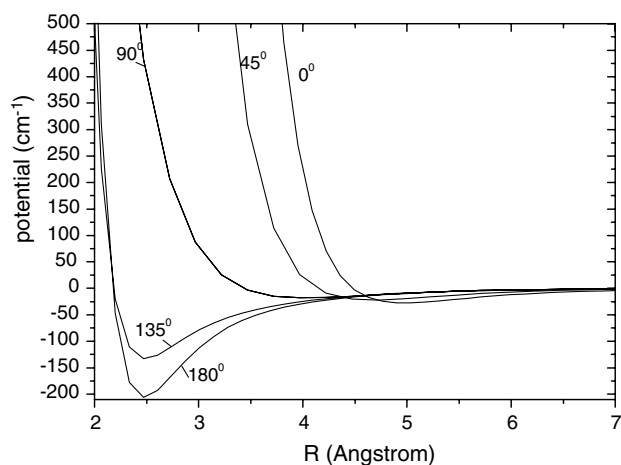


Fig. 1. Sections of the Ne–LiH potential energy surface associated with five different Jacobi angles.

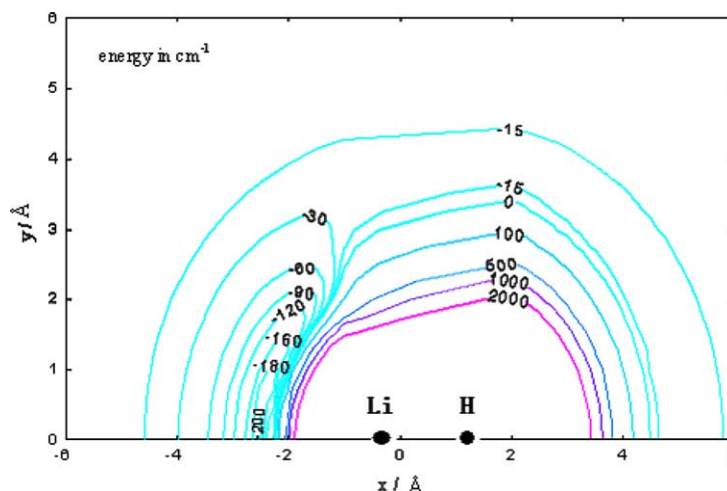


Fig. 2. Equipotential energy contours of the Ne–LiH potential as a function of the distance of the Ne from the LiH center of mass.

sponding to the linear Ne–HLi) with a well depth of 27.34 cm^{-1} (not shown in Fig. 2). Compared with the He–LiH system, the global minimum of Ne–LiH potential is deeper than that of He–LiH, the latter is 179.9 cm^{-1} for MP4 [6] and 176.7 cm^{-1} for CCSD(T) [5].

2. The interaction potential is highly angular anisotropic, similar to that of He–LiH system. At $\theta < 90^\circ$ the potential is essentially repulsive except the shallow well at 4.97 \AA , while at $\theta > 90^\circ$, the attractive well becomes pronounced. This character stems from the electronic structure of the LiH molecule, which can be viewed as a Li^+H^- ion pair state. The large electron dipole moment [3] leads to the strong anisotropy of the induction forces. When the Ne atom is near the lithium end of LiH, it is strongly attracted to the compact Li^+ core under the influence of induction forces. In principle, the same forces are active at the hydrogen end of LiH, however, Pauli repulsion between the Ne atom and the diffuse H^- electron cloud forces the Ne atom to move away from LiH. In order to accommodate this extreme angular anisotropy of the potential, the expanding of the potential in Legendre polynomials (see Eq. (5) below) must include enough terms.

2.2. The quantum dynamics

In our work we implement the CC calculation for rotationally inelastic collision of LiH with Ne. This may be done either in a Body-fixed frame [14] or in a Space-fixed (SF) [15] frame. In order to obtain the experimental observations such as differential cross-section and temperature-dependent rate constant, the SF frame is a favorable one. We use the conventional Jacobi coordinates (R, r, θ) , where r is the bondlength of LiH (fixed at its equilibrium value, 1.595 \AA), R is the separation of the atom Ne and the center of mass of LiH, and θ is the enclosed angle, $\theta = 0^\circ$ corresponds to the collinear Ne–HLi geometry. Because of the nonspherical nature of the interaction, the usual coupled angular momentum representation prove to be more efficient, namely

$$\phi_{jl}^{JM}(\hat{R}, \hat{r}) = \sum_{m_j m_l} \langle jlm_j m_l | jJM \rangle Y_{lm_l}(\hat{R}) Y_{jm_j}(\hat{r}), \quad (1)$$

where J denotes the total angle momentum, j the rotational angle momentum for LiH, and l the orbital angular momentum, respectively. The total scattering wavefunction is expanded as

$$\psi_{jl}^{JM}(\hat{R}, \hat{r}) = \sum_{j'l'} R^{-1} u_{j'l'}^{Jl}(R) \phi_{j'l'}^{JM}(\hat{R}, \hat{r}). \quad (2)$$

It is seen from Eq. (2) that the presence of the two sets of asymptotic indices (jl) and $(j'l')$ prepares for a representation of the effect of the anisotropic potential which will couple the initial state (jl) with the final state $(j'l')$.

Substitution of Eq. (2) into stationary Schrödinger equation, the CC equations for the radial coefficients $u_{j'l'}^{Jl}$ are resulted as

$$\left(\frac{d^2}{dR^2} + k_{j'l'}^2 - \frac{l'(l'+1)}{R^2} \right) u_{j'l'}^{Jl}(R) = 2\mu \sum_{j''l''} \langle j'l' | V(R, \theta) | j''l'' \rangle u_{j''l''}^{Jl}(R) \quad (3)$$

with

$$k_{j'l'}^2 = 2\mu(E_{\text{col}} + \varepsilon_{\text{rot}}^j - \varepsilon_{\text{rot}}^{j'}), \quad (4)$$

where E_{col} is the collision energy, $\varepsilon_{\text{rot}}^j$ and $\varepsilon_{\text{rot}}^{j'}$ are the initial and final rotational energy levels of LiH, respectively. The interaction potential is conventionally expanded in Legendre polynomials such as

$$V(R, \theta) = \sum_{\lambda} V_{\lambda}(R) P_{\lambda}(\cos \theta), \quad (5)$$

so that the angular integrals $\langle j'l' | P_{\lambda}(\cos \theta) | j''l'' \rangle$ can be taken analytically [7].

The coupled Eq. (3) are solved numerically. Matching the solutions to the proper boundary conditions for the radial wavefunction ($u_{j'l'}^{Jl}$) in the asymptotic region leads to the transition matrix elements $T_{jl \rightarrow j'l'}^J$. The scattering amplitude is taken as [16]

$$f_{jm_j \rightarrow j'm_{j'}}(\hat{R}) = \left(\frac{\pi}{k_j k_{j'}} \right)^{1/2} \sum_{J M l' m_{l'}} i^{l'-l'+1} (2l+1)^{1/2} \times \langle j'm_{j'} l' m_{l'} | j'l' J M \rangle \times T_{jl \rightarrow j'l'}^J \langle jlm_j 0 | jJM \rangle Y_{l'm_{l'}}(\hat{R}), \quad (6)$$

from which the differential cross-sections for the $j \rightarrow j'$ transition averaged over initial m_j and summed over final $m_{j'}$ projections, are:

$$\frac{d\sigma_{j \rightarrow j'}}{d\Omega} = \frac{k_{j'}}{(2j+1)k_j} \sum_{m_j m_{j'}} \left| f_{jm_j \rightarrow j'm_{j'}} \right|^2. \quad (7)$$

The total cross-sections are given by the usual formulae

$$\sigma_{j \rightarrow j'} = \sum_J P_{j \rightarrow j'}^J, \quad (8)$$

here, $P_{j \rightarrow j'}^J$ stands for the partial cross-section

$$P_{j \rightarrow j'}^J = \frac{(2J+1)\pi}{(2j+1)k_j^2} \sum_{l'l'} \left| T_{jl \rightarrow j'l'}^J \right|^2. \quad (9)$$

Since the T matrix goes to zero for large J , this sum will converge and can be truncated.

3. Results and discussions

In our calculations the hybrid modified log-derivative Airy propagator [17] is used to solve the CC equations and obtain rotationally inelastic cross-sections. From $R = 1.5 \text{ \AA}$ to $R = 8 \text{ \AA}$ the log-derivative propagator is

used, while from $R = 8 \text{ \AA}$ to $R = 15 \text{ \AA}$ the Airy propagator is used. The rotational basis sets include all the energetically open rotational channels and at least two energetically closed channels at each collision energy. The sum over total angular momentum J terminate when the inelastic integral cross-sections is converged to better than 0.02 \AA^2 and the elastic cross-sections to within 1 \AA^2 . Twenty-four point Gauss–Legendre quadrature is adopted to evaluate the expansion coefficients $V_\lambda(R)$ in Eq. (5), and the Legendre terms up to $\lambda_{\text{max}} = 12$ are included. The results are checked by reasonable change in the propagator step size, the maximum distance for the propagation and the total number of rotational states included in the basis.

3.1. Differential cross-sections

We try first to understand some features of the Ne–LiH collision by looking at inelastic differential cross-sections (DCS). DCS can be directly measured by a crossed molecular beam experiment, the number of ro-vibrationally selected LiH molecule striking a finite size detector at a fixed scattering angle will be proportional to DCS.

In Fig. 3 we show the computed state-to-state rotational DCS of Ne–LiH system from the initial $j = 0$ at a collision energy of 1000 cm^{-1} (refer to the $j = 0$ rotational level of LiH molecule). The fast narrow diffraction oscillations in the cross-sections are the obvious characters for the low Δj inelastic transitions, which

decrease with j' increasing. It is well known that they are resulted from the interference of quantum mechanical waves, which are associated with different classical trajectories that lead to the same scattering angle and angular momentum transfer. The largest amplitude occurs at small scattering angles. There is very little backward scattering. This suggests that at a low Δj transition, the Ne projectile is predominantly forward scattering in the molecular frame of reference. This is not surprising since only 14.8, 44.4, 88.7 and 147.8 cm^{-1} of energy is required to support the $j = 0$ to $j' = 1$ –4 transition, respectively; it only requires a “glancing blow” (corresponding to larger impact parameter) to provide these energies for a collision at $E_{\text{col}} = 1000 \text{ cm}^{-1}$. For such collision, the particles will continue their journey after excitation, thus, we will find the particles in the forward directions.

For purely repulsive potentials, the previous studies [18–20] showed that the angular distributions of inelastic DCS provide a useful visualization of rotational rainbows, which possess the following typical characteristics: they are “dark”, i.e., low intensity, at the low angle side of the rainbow. However, when the low Δj inelastic transitions are considered, it is obviously not the case as described above here. For $\Delta j \leq 4$ in the Ne–LiH system, the main rainbow maximum is completely buried under the forward diffraction oscillations and one almost cannot find any distinct rainbow structure. This behavior is a reflection of the fact that the PES of Ne–LiH system possess attractive well, which exhibits strong

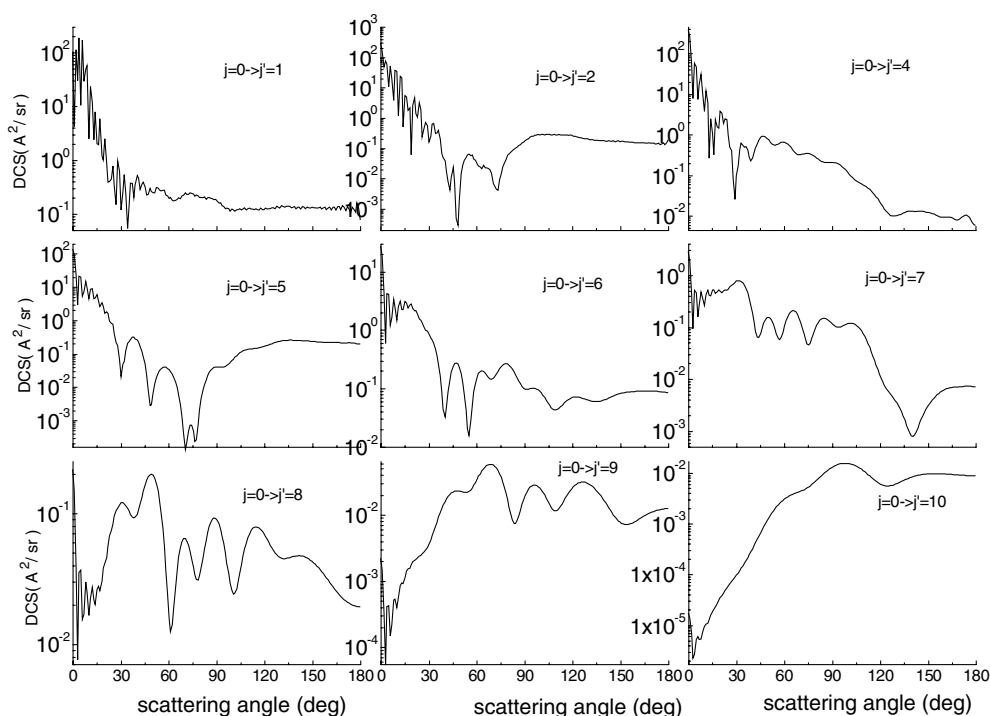


Fig. 3. State-to-state differential cross-sections for Ne + LiH ($j = 0$) at a center of mass collision energy of 1000 cm^{-1} .

anisotropy. Similar behavior has been seen for He–HF and He–LiH scattering [19]. It is therefore reasonable to suggest that attractive well plays a considerable role at low Δj inelastic collisions.

As j' increases from 5 to 10, the amplitudes of the diffraction oscillations at the small scattering angles decrease successively and disappear completely at $j' = 10$. Simultaneously, the rotational rainbow structure becomes progressively distinct. The main rotational rainbow emerges at the forward scattering angle, and its position shifts to higher scattering angles as the rotational inelasticity increases. There are also several wider supernumerary oscillations in the bright-side of the main rainbow. In common with rotational inelastic scattering of many other systems, the large amplitude of DCS spans a wide angular region from forward to backward scattering. Classically, these characteristics correspond to scattering off the hard repulsive core of the PES, which can impart significant torque and hence induce rotational excitation. It can be understood by inspecting the contours presented in Fig. 2. Because of “kinks” existing in the Li end on the PES, while the incoming Ne atom strike LiH from this end, the kinks in the positive energy contours at $\theta \geq 90^\circ$ offer the greatest chance for Ne projectile to exert a torque on the LiH molecule. Since the potential is strongly attractive at this end, these types of trajectories should be favorable for considerably large rotational DCS in the backward scattering [20].

3.2. Partial cross-sections

We can also better understand the collisional energy transfer process by inspection of the contribution of each partial wave to the total cross-section. In Fig. 4, we show the representative partial cross-sections from ini-

tial state $j = 0$ to final state j' at collision energy 500 cm^{-1} . Once again we see interference patterns due to coupling between the Ne orbital momentum l and the LiH rotational angular momentum j . The typical character of the curves is that there are two peaks for each inelastic transition. Since the molecule is initially in ground rotational state $j = 0$, the total angular momentum J equals the orbital angular momentum of the incoming channel, therefore, these plots also represent partial cross-sections as function of initial orbital angular momentum l . Classically, impact parameter can be associated with a given l using the relation

$$b_l \sim l / \sqrt{2\mu E}. \quad (10)$$

It is found from Eq. (10) that $b_{30} = 2.2 \text{ \AA}$, $b_{42} = 3.2 \text{ \AA}$, $b_{55} = 4.2 \text{ \AA}$ for $E = 500 \text{ cm}^{-1}$, and $b_{40} = 2.2 \text{ \AA}$, $b_{60} = 3.2 \text{ \AA}$, $b_{78} = 4.2 \text{ \AA}$ for $E = 1000 \text{ cm}^{-1}$. Combined with Fig. 1 and Fig. 2 one sees that orbital angular momentum from 0 to 30 therefore correspond to scattering off the repulsive wall of the potential; from 30 to 55 correspond to collisions with impact parameters in the region where both the attractive and repulsive part of the potential contribute to the partial cross-sections. For $l > 55$ the scattering is determined mainly by the attractive tail of the potential.

Based on the above argument, we suggest a reasonable interpretation of the behavior of the collision dynamics shown in Fig. 4 as follow. Hard, or repulsive, collision, in which the Ne atom bounces off the repulsive core of the LiH molecule, accounts for the peak between $J = 0$ and $J = 30$ appeared in cases of final $j' \geq 3$, and contributes the most of the DCS for large scattering angle. When the impact parameters increase to make the Ne atom completely missing the repulsive part of the PES, the interaction with the attractive part in the long-range of the PES is also able to couple the rotation of

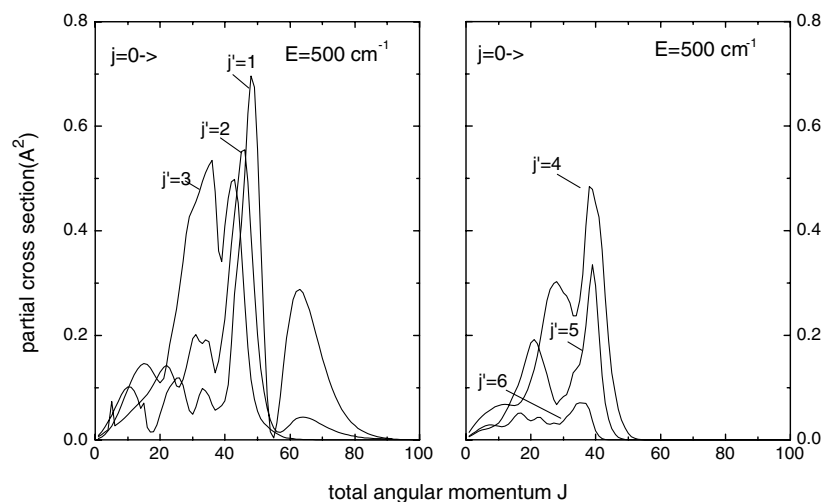


Fig. 4. State-to-state partial cross-sections from initial state $j = 0$ to final state j' as functions of total angular momentum at collision energy of 500 cm^{-1} .

LiH molecule with the relative translation, and thus contributes to the partial cross-sections. This mechanism is responsible for the partial cross-sections for $J > 55$, which is very efficient at exciting LiH molecule from $j = 0$ to $j' = 1$. It is interesting to note that from Eq. (10) we obtain an impact parameter corresponding to the peak at $J = 65$ as $b_{65} = 4.98 \text{ \AA}$, which is just the location of the shallower well in the H side. This means that the Ne atom attacks the LiH molecule from the H side, thus, the attractive well in the long-range of PES also plays a considerable role in determining the DCS in the forward scattering of low Δj inelastic transition, as is discussed for Fig. 3. As for the impact parameters in the range of $2.2 < b < 4.2 \text{ \AA}$, collision sample both the repulsive and attractive part of PES, and the curve are the net contributions resulted from the two parts. For the J values of 30–42, the short-range attractive well in the Li side of the potential also contributes considerable quantity of partial cross-sections, except the contributions from repulsive part; J values of 42–55 correspond to the collisions sampling the region where the repulsive property of the potential has predominance over attractive property, on which the peak at $J \approx 50$ appearing in inelastic transition from $j = 0$ to $j' = 1, 2$ and 3 is understandable. When J arrive at 55, the net contributions attain its minimum.

Fig. 5 shows the partial cross-sections for the same rotational transitions as in Fig. 4 but at collision energy 1000 cm^{-1} . One can see that the behavior of the partial cross-sections as function of the total angular momentum J is similar to the case of $E = 500 \text{ cm}^{-1}$ shown in Fig. 4. For example, although the positions of the two peaks and of the minimum in inelastic transition $j = 0 \rightarrow j' = 1$ are different in two cases, but they correspond to almost equal impact parameters, namely $b_{50} = 3.83 \text{ \AA}$, $b_{55} = 4.21 \text{ \AA}$, $b_{65} = 4.98 \text{ \AA}$ for $E = 500$

cm^{-1} , and $b_{70} = 3.80 \text{ \AA}$, $b_{78} = 4.21 \text{ \AA}$, $b_{90} = 4.90 \text{ \AA}$ for $E = 1000 \text{ cm}^{-1}$, which means that they sample the same portion of the PES, respectively. As the collision energy increases, the Ne atom penetrates the potential deeper, so the value of impact parameters related to the peaks decreases slightly. In addition, we see again that the long-range attractive well makes its significant contribution to the partial wave cross-sections for lower Δj inelastic transitions, whereas as if it does not exist for the higher inelastic transitions, as seen from Fig. 4. Thus, we consider the interpretation of the collision dynamics for $E = 1000 \text{ cm}^{-1}$ in Fig. 5 is similar to that for $E = 500 \text{ cm}^{-1}$ in Fig. 4.

3.3. Integral cross-sections

The inelastic CC $j = 0, 1 \rightarrow j'$ integral cross-sections are listed in Table 1 and the values are displayed graphically in Fig. 6. We notice first that a fairly large range of occupied final rotational state j' exists, which decreases in general with increasing j' . This trend is what expected for surfaces characterized by high orientational anisotropy; even the large Δj transitions are directly coupled by Legendre terms in Eq. (5). Another interesting property in Fig. 6 is that the cross-sections exhibit an oscillatory rather than monotonic behavior with increasing Δj . This structure, which has also been observed in calculations of integral rotationally inelastic cross-sections for other weakly interacting molecular system such as He–LiH [21] and $\text{Li}^+ - \text{CO}$ [22], are often classified as rotational rainbow structure in the integral cross-sections, compared to the “rotational rainbow” in rotationally inelastic DCS. It is obvious from Fig. 6 that the general shapes of the curve in two cases are similar to each other, but the positions of oscillatory feature change dramatically with collision energy: the undula-

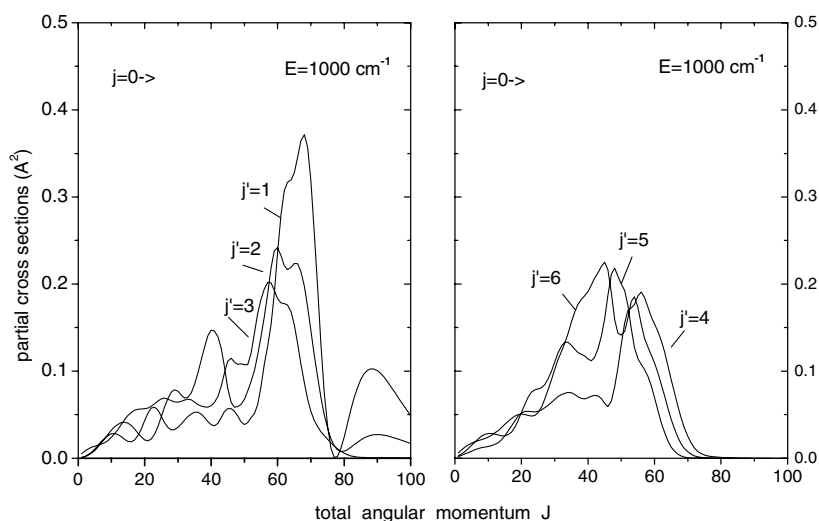


Fig. 5. State-to-state partial cross-sections from initial state $j = 0$ to final state j' as function of total angular momentum at collision energy of 1000 cm^{-1} .

Table 1

Integral state-to-state cross-sections $\sigma_{jj'}$ (\AA^2) for the transition from the initial rotational state $j = 0, 1$ to the final rotational state j' at collision energies of 1000 and 2000 cm^{-1}

j'	$E = 1000 \text{ cm}^{-1}$		$E = 2000 \text{ cm}^{-1}$	
	$j = 0$	$j = 1$	$j = 0$	$j = 1$
0	83.64	3.01	60.8	2.57
1	8.89	87.33	7.64	63.47
2	7.58	8.49	6.00	6.95
3	6.10	6.85	4.34	5.25
4	5.10	5.81	3.85	4.24
5	6.66	6.47	3.50	3.61
6	5.64	5.78	3.38	3.31
7	3.27	3.40	2.85	3.02
8	1.37	1.46	3.06	3.10
9	0.37	0.40	3.35	3.34
10	0.10	0.11	2.54	2.56
11	0.005	0.005	1.19	1.24
12			0.43	0.46
13			0.15	0.16
14			0.06	0.06
15			0.02	0.02
16			0.00	0.00

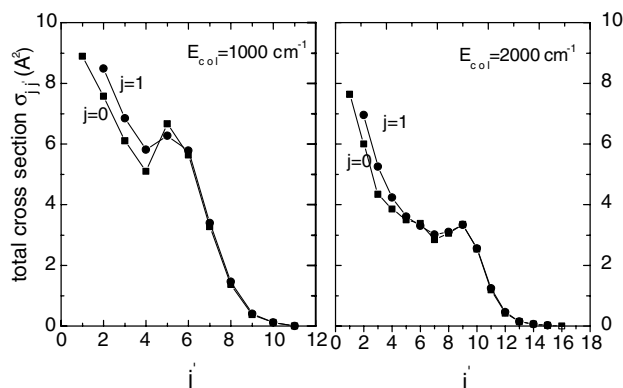


Fig. 6. Inelastic state-to-state integral cross-sections for Ne + LiH ($j = 0, 1$) as function of the final rotational state j' at collision energies of 1000 and 2000 cm^{-1} , respectively.

tory peak takes place at $j' = 5$ for collision energy of 1000 cm^{-1} and shifts to $j' = 9$ for collision energy of 2000 cm^{-1} . This undulatory structure could well prove to be a sensitive probe of the interaction potential [21].

In Fig. 7, we show the low energy CC $j = 0 \rightarrow j'$ cross-sections as a function of collision energy. Over the energy range shown, collision populates rotational levels up to $j' = 3$. There are relatively sharp resonance features in the $j = 0 \rightarrow 1, 2$ cross-sections. These resonances are believed to be resulted from quasi-bound states arising from the Ne being temporarily “stuck” to the LiH. Because a slower Ne atom has much time stick to the LiH, the amplitude of these peaks increases at lower collision energies. Since the potential surface for Ne–LiH has a substantially deeper minimum than that presented in [4] for He–LiH system, it is not sur-

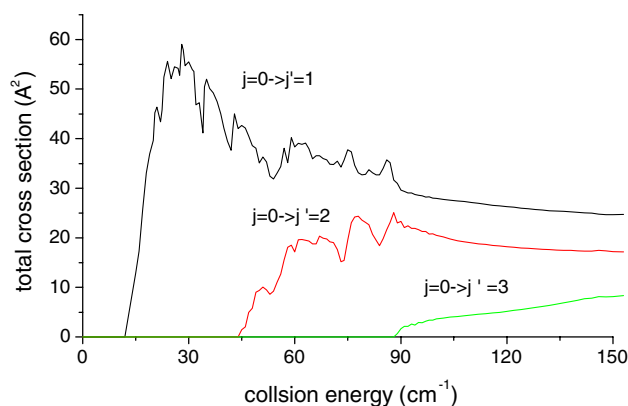


Fig. 7. Low energy CC $j = 0 \rightarrow j'$ cross-sections as function of collision energy.

prising that these resonances are visible in our cross-sections but disappear in [7] (Fig. 8). In addition, these resonances can also be seen in [5] (Fig. 5), which is based on a more attractive surface at the CCSD(T) level for He–LiH complex. In fact, the calculation of the energy level showed indeed that the potential used in our work support three bound vibrational states [13].

4. Conclusions

In this work, we have employed a newly computed potential energy surface to study various state-to-state cross-sections of the rotationally inelastic excitation of LiH molecule by collision with Ne atom. The close coupling method is adopted. Differential cross-sections show the feature of forward scattering in low Δj inelastic transitions and backward scattering in high Δj . Two maxima exist in the curve of partial cross-sections, and they are originated from different mechanism. The long-range attractive well makes the significant contribution to the partial cross-sections for $j = 0 \rightarrow j' = 1, 2$ inelastic transitions, whereas as if it does not exist for higher inelastic transitions. The dependence of the integral cross-sections on j' for initial $j = 0, 1$ displays a pronounced oscillatory structure rather than a monotonic one, which prove to be a sensitive probe of the interaction potential. The dependence on low collision energy presents resonance features. We relate these features to the anisotropic interaction potential. We hope that this work can provide useful information for further experimental and theoretical studies.

Acknowledgements

Thanks are due to Professor Xie for providing a FORTRAN subroutine generating the Ne–LiH interaction potential. This work supported by the Natural Science Foundation of Anhui educational committee

(Grant 2003kj169). We appreciate the referee for helpful suggestions for improvement of the manuscript.

References

- [1] A. Dalgarno, K. Kirby, P.C. Stancil, *Astrophys. J.* 458 (1996) 397.
- [2] F.A. Gianturco, F. Paesani, R. Curik, G. Delgado-Barrio, T. Gozalez-Lezana, S. Miret-Artes, P. Villareal, *Chem. Phys. Lett.* 311 (1999) 255.
- [3] D.M. Silver, *J. Chem. Phys.* 72 (1980) 6445.
- [4] F.A. Gianturco, S. Kumar, S.K. Pathak, M. Raimondi, M. Sironi, *Chem. Phys.* 215 (1997) 227.
- [5] B.K. Taylor, R.J. Hinde, *J. Chem. Phys.* 111 (1999) 973.
- [6] G.S. Yan, M.H. Yang, D.Q. Xie, *Sci. China (B)* 40 (1997) 554.
- [7] F.A. Gianturco, S. Kumar, S.K. Pathak, M. Raimondi, M. Sironi, *Chem. Phys.* 215 (1997) 239.
- [8] A. Forni, *J. Mol. Struct. (THEOCHEM)* 468 (1999) 73.
- [9] S.S. Bhattacharyya, A.S. Dickinson, D. Richards, *J. Phys. B* 12 (1979) 595.
- [10] B.E. Wilcomb, P.J. Dagdigian, *J. Chem. Phys.* 67 (1977) 3829.
- [11] D.W. Davies, *Chem. Phys. Lett.* 112 (1984) 142.
- [12] A.S. Shalabi, M.M. Assem, S. Abdel-Aal, M.A. Kamel, M.M.A. El-Rahman, *Solid State Commun.* 111 (1999) 735.
- [13] Yuhui Lu, Daiqian Xie, Minghui Yang, Guosen Yan, *Chem. Phys. Lett.* 327 (2000) 305.
- [14] J.M. Launay, *J. Phys. B* 10 (1977) 3665.
- [15] A.M. Arthurs, A. Dalgarno, *Proc. Roy. Soc. A* 256 (1963) 540.
- [16] W.H. Miller (Ed.), *Dynamics of Molecular Collisions*, vol. 1, Plenum Press, New York, 1976, p. 13.
- [17] D.E. Manolopoulos, M.H. Alexander, *J. Chem. Phys.* 86 (1987) 2044.
- [18] Leslie J. Rawluk, Y.B. Fan, Y. Apelblat, Mark Keil, *J. Chem. Phys.* 94 (1991) 4025.
- [19] F.A. Gianturco, A. Palma, *J. Chem. Phys.* 83 (1985) 1049.
- [20] P.F. Vohralik, R.E. Miller, R.O. Watts, *J. Chem. Phys.* 90 (1988) 2182.
- [21] E.F. Jendrek, M.H. Alexander, *J. Chem. Phys.* 72 (1980) 6452.
- [22] L.D. Thomas, *J. Chem. Phys.* 67 (1977) 5224.